BIOCHEMISTRY
including biophysical chemistry & molecular biology
Article

Biochemistry **XXXX,** *XXX,* 000–000 A
DOI: 10.1021/bi901090m

Conformational Changes Specific for Pseudophosphorylation at Serine 262 Selectively Impair Binding of Tau to Microtubules†

Daniela Fischer,‡ Marco D. Mukrasch,‡ Jacek Biernat,§ Stefan Bibow,‡ Martin Blackledge,∥ Christian Griesinger,‡ Eckhard Mandelkow,§ and Markus Zweckstetter*,‡,⊥

‡*Department for NMR-Based Structural Biology, Max Planck Institute for Biophysical Chemistry, Am Fassberg 11, 37077 Göttingen, Germany,* ⊥*DFG Research Center for the Molecular Physiology of the Brain (CMPB), Göttingen, Germany,* ∥*Institut de Biologie Structurale Jean-Pierre Ebel, CEA-CNRS-UJF UMR 5075, 41 Rue Jules Horowitz, Grenoble 38027, France, and* §*Max Planck Unit for Structural Molecular Biology, c/o DESY, Notkestrasse 85, 22607 Hamburg, Germany*

Received June 29, 2009; Revised Manuscript Received September 18, 2009

ABSTRACT: Aggregation of the microtubule-associated protein tau into neurofibrillary tangles is the pathological hallmark of a variety of dementias. For reasons not yet known, tau becomes excessively phosphorylated in Alzheimer's brains and as a result no longer binds properly to microtubules. Here we studied the impact of phosphorylation on the conformational and binding properties of the repeat region of tau (K18) that is necessary for microtubule assembly and forms the core of paired helical filaments. To mimic phosphorylation, we introduced four mutations of serine to glutamate residues at positions 262, 293, 324, and 356. NMR spectroscopy demonstrates that pseudophosphorylation at these sites modifies the structural properties in repeats 1 and 2, in particular for Gln265−Lys267. Gln265−Lys267 are in close proximity to Ser262, the phosphorylation site that most strongly attenuates binding to microtubules. In contrast, the pseudophosphorylation mimic of tau efficiently interacts with the polyanion heparin. Thus, phosphorylation of the repeat region of natively unfolded tau induces specific conformational changes that have a strong impact on its biological function and involvement in disease.

Alzheimer's disease (AD)[1] is the most common dementia affecting aging societies. The impairment of cognitive function in patients suffering from this disease is accompanied by the occurrence of two types of protein aggregates: extracellular plaques made up by the β-amyloid peptide and intracellular "neurofibrillary tangles" comprising the protein tau (*1*). During the past decade overall interest focused on Aβ as the decisive factor causing the occurrence of AD. However, several observations made during recent years indicate that tau plays an important role in the cognitive impairment of AD patients (*2*).

Tau is a microtubule- (MT-) associated protein that exists in six different isoforms in the human central nervous system. The isoforms differ by two inserts near the N-terminal end and the presence of either four or three imperfect repeat sequences in the C-terminal half of the protein (Figure 1A). The repeat domain represents the core of the MT interaction (*3*−*5*) and also forms the core of paired helical filaments (PHFs) (*6*, *7*). For aggregation into PHFs two hexapeptides at the beginning of the second and third repeats (^{275}VQIINK^{280} and ^{306}VQIVYK^{311}) are crucial because they are able to initiate the aggregation process by forming β-structure (*8*).

At least 30 phosphorylation sites in PHF tau have been identified (for a review see ref *9*). Phosphorylation of tau can lead to detachment of tau from MTs, MTs become destabilized, and the unbound tau is free to undergo abnormal aggregation. *In vivo*, hyperphosphorylation of tau precedes tangle formation (*10*−*12*) and in *Drosophila* models, neurodegenerative effects appear not to depend on tau tangles but rather on increased phosphorylation of tau (*13*). The protein kinase MARK can phosphorylate several sites within the repeats (notably the KXGS motifs including Ser^{262}, Ser^{324}, and Ser^{356}) (*14*, *15*). Phosphorylation at these sites appears early in AD (*16*), MARK protein is elevated in neurofibrillary tangles in AD brain (*17*), and MARK phosphorylation sites on tau are elevated early in transgenic mouse models of tauopathy (*18*). However, it is still unclear which kinases are responsible for phosphorylation of tau *in vivo* and how phosphorylation of tau is linked to its aggregation and neuronal degeneration observed in disease.

Tau is a prototypical "natively unfolded" protein that does not assume a rigid tertiary or secondary structure but populates an ensemble of interconverting structures in solution (*3*, *19*). Due to their inherent flexibility, natively unfolded proteins are not amenable for structure analysis by crystallography. Thus nuclear magnetic resonance (NMR) spectroscopy is the only method that allows a description of their conformations and dynamics with high resolution (*20*). NMR studies have already revealed interesting insights into the structural properties of soluble tau and PHF tau (*7*, *21*−*28*). We have recently shown that it is possible to obtain the complete backbone resonance assignment of the longest isoform of human tau and demonstrated that 441-residue tau has a distinct domain character with an intricate network of

†This work was supported by the Max Planck Society and through a DFG Heisenberg scholarship to M.Z. (ZW 71/2-1 and 3-1).

*To whom correspondence should be addressed. E-mail: mzwecks@gwdg.de. Tel: ++49 551 201 2220. Fax: ++49 551 201 2202.

[1]Abbreviations: AD, Alzheimer disease; MARK, microtubule-associated protein−microtubule affinity regulating kinase; K18, four-repeat domain of tau; K18wt, wild-type K18; K18-4×KXGE, pseudophosphorylation mutant of K18; PHF, paired helical filament; MT, microtubule; CD, circular dichroism; NMR, nuclear magnetic resonance; HSQC, heteronuclear single-quantum coherence; RDC, residual dipolar coupling.

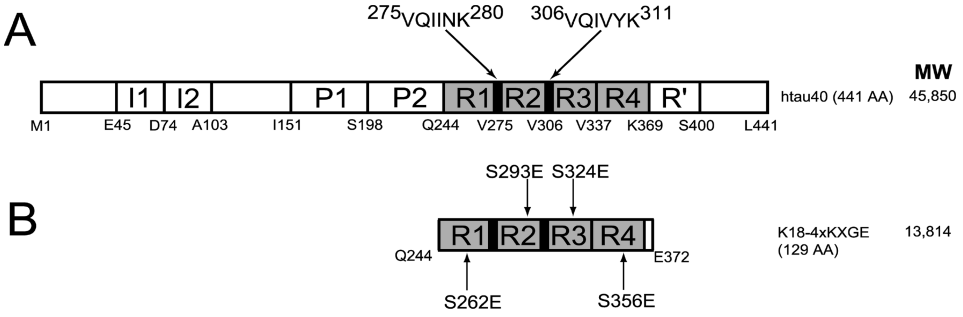

FIGURE 1: Tau protein, the repeat domain, and KXGE mutations. (A) The longest isoform of tau (441 residues) in the human central nervous system. The C-terminal half contains three or four pseudorepeats (~31 residues each, R1 to R4). Repeat 2 and the two near-N-terminal inserts (I1, I2) may be absent due to alternative splicing. The positions of the aggregation-prone hexapeptide motifs ^{275}VQIINK^{280} and ^{306}VQIVYK^{311} in repeats R2 and R3 are highlighted. (B) Construct K18 (130 residues, (M)Q244-E372) comprises only the four repeats. To mimic phosphorylation, the four serine residues of the KXGS motifs (residues 262, 293, 324, and 356 in repeats R1, R2, R3, and R4, respectively) were mutated into glutamic acid. Numbering of residues follows that of the longest isoform.

transient long-range contacts (*3*). Homonuclear NMR studies of short peptides of tau suggested that phosphorylation causes changes in the local conformation (*29*); in particular, turns (*30*) or type II polyproline helical structures (*31*) might be induced in the proline-rich region and affect the rate of proline isomerization (*30*, *32*).

Here we applied heteronuclear NMR spectroscopy to obtain insight into the impact of phosphorylation on the structural properties of the repeat region of tau, as well as its influence on the interaction with microtubules and the aggregation inducer heparin. To reduce NMR signal overlap but at the same time allow cross-talk between different phosphorylation sites, we used a 130-residue fragment of tau (K18), in which all four repeats of tau are present (Figure 1) (*23*). To overcome the problem of low specificity of protein kinases, we mimic phosphorylation by mutation of the serine residues of the KXGS motifs (residues 262, 293, 324, and 356 in repeats R1, R2, R3, and R4, respectively) to glutamic acid (Figure 1). Although this approach is unlikely to completely mimic phosphorylative changes, it was previously demonstrated to imitate effects of phosphorylation (*33*, *34*).

MATERIALS AND METHODS

Expression of Recombinant Tau Constructs and Isotope Labeling. The single mutation S262E and the four KXGE mutations in the construct K18 (residues Q244−E372 of the longest tau isoform in the human brain plus initial M243, 130 residues) were created by site-directed mutagenesis using the QuickChange kit (Stratagene, Amsterdam, The Netherlands). The constructs are named K18-S262E and K18-4×KXGE, respectively. The introduced modifications were verified by DNA sequencing. Expression, purification, and isotope labeling were performed as described previously (*23*). NMR samples contained 2 mM ^{15}N-labeled protein in 95% H_2O/5% D_2O and 50 mM phosphate buffer, pH 6.8, with 1 mM dithiothreitol.

Preparation of MTs. Porcine brain tubulin was purified as described and incubated at concentrations higher than 200 μM in MT assembly buffer (100 mM Pipes, pH 6.9, 1 mM EGTA, 1 mM $MgSO_4$, 1 mM DTT) in the presence of 1 mM GTP at 37 °C for 5 min. After the addition of 100 μM paclitaxel (Sigma-Aldrich Chemie, Munich, Germany) the polymerization was performed for 20 min at 37 °C.

CD Spectroscopy. All measurements were carried out with a Jasco J-715 CD spectrometer (Jasco, Gross-Umstadt, Germany) in a cuvette with a path length of 0.1 cm. The spectra were recorded between 190 and 240 nm at a scanning speed of 100 nm/min, a bandwidth of 1.0 nm, and a response time of 0.5 s. In each experiment, three spectra were summed and averaged. For calculation of the mean residue ellipticity, the protein concentration was obtained by using the second channel of the CD spectrometer and measuring the absorption of the protein sample at 214 nm (where absorption is dominated by the peptide bonds). Calibration at 214 nm was done with a BSA standard.

NMR Spectroscopy. NMR spectra were acquired at 5 °C on Bruker Avance 700, Avance 600, and DRX 600 spectrometers. Aggregation did not occur at 5 °C in the absence of polyanions. NMR data were processed and analyzed using NmrPipe (*35*) and Sparky 3 (www.cgl.ucsf.edu/home/sparky/). Three-dimensional triple-resonance experiments (HNHA (*36*) (F1:80 × F2:150 × F3:1K complex points) and NOESY-HSQC (*37*) (F1:320 × F2:120 × F1:1K complex points)) were collected to obtain sequence-specific assignments for the backbone of K18-4×KXGE. Secondary chemical shifts from natural abundance HNCO (*38*) (F1:80 × F2:56 × F3:1K complex points) and HNCA (*38*) (F1:80 × F2:56 × F3:1K complex points) experiments were calculated using NMRView (*39*) as the difference between the measured Cα/C′ chemical shifts and the empirical, sequence-corrected random coil values (*40*, *41*) for the appropriate amino acid type at pH 2.3. Random coil values for the pH-sensitive residues histidine, glutamate, and aspartate were taken from Wishart et al. (*41*) for a better accordance of the pH value and our experimental conditions. Random coil values for residues preceding Pro were taken from Wishart et al. (*42*).

One-bond N−H RDCs (D_{NH}) (*43*) were determined by using the 2D inphase−antiphase (IPAP)-HSQC experiment (*44*). D_{NH} values were calculated as the difference between splittings measured in the isotropic phase and in a sample, in which K18-S262E or K18-4×KXGE had been aligned in 5 mg/mL Pf1 bacteriophage (Asla, Riga, Latvia) (deuterium splitting 2.2 Hz). RDCs were not corrected for the negative gyromagnetic ratio of ^{15}N.

Tau−heparin titrations were carried out at pH 6.8 using uniformly ^{15}N-labeled protein containing 150 μM K18-4×KXGE in 50 mM phosphate buffer, respectively. Heparin (average molecular weight 3350, 5.8 disaccharide subunits, charge/subunit −2.5, −0.31 z/Å) was purchased from Sigma. The formation of the tau−heparin complex was studied by 2D ^{1}H−^{15}N HSQC spectra using a tau:heparin ratio of 1:2.

For tau−MT titrations the samples contained 150 μM uniformly ^{15}N-labeled K18-4×KXGE in MT assembly buffer.

Complex formation was monitored at 5 °C for MT concentrations ($\alpha\beta$-tubulin dimers) of 150 μM. Previous experiments including sedimentation, SDS−PAGE, and electron microscopy on K18 and K19 wild-type protein had already shown that MTs in the paclitaxel-stabilized form are stable at 5 °C during the time course of the NMR measurements (*23*).

RESULTS

Backbone Resonance Assignment of K18-4×KXGE. The circular dichroism spectra of wild-type K18 (K18wt) and the pseudophosphorylation mimic K18-4×KXGE were very similar, suggesting that the mutations did not result in formation of rigid secondary structure (Figure 2). Moreover, a two-dimensional

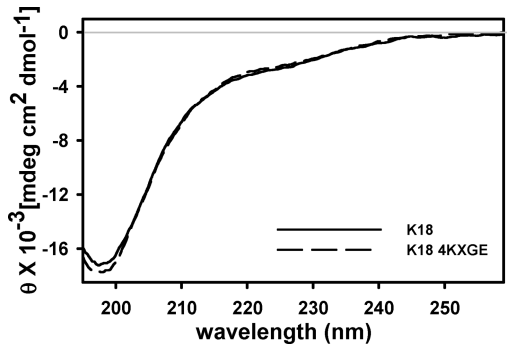

FIGURE 2: Circular dichroism of K18wt (—) and K18-4×KXGE (- - -) at 20 °C. The molecular ellipticity was plotted vs the wavelength.

^{1}H−^{15}N HSQC spectrum of K18-4×KXGE exhibited sharp resonances with a congestion of signals due to the protein's intrinsically disordered nature (Figure 3A). Starting from the assignment of K18wt, which was previously determined by us (*23*), it was possible to assign the mutant protein by three-dimensional HNHA, NOESY-HSQC, HNCO, and HNCA spectra. The PGGG sequence motifs could not be assigned unambiguously due to strong signal overlap in the glycine region similar to the assignment of the wt protein (this accounts for the gaps in Figure 3 and following). Furthermore, an unambiguous assignment of Glu^{262}, Glu^{293}, Glu^{324}, and Glu^{356} could not be achieved. For all other residues of K18-4×KXGE the ^{1}H, ^{15}N, ^{13}Cα, and ^{13}C′ chemical shifts were assigned. Changes in the ^{15}N and ^{1}H chemical shifts were pronounced in the vicinity of the mutations, in particular in repeat R1 close to Glu^{262} (Figure 3B,C).

Residual Secondary Structure. NMR chemical shifts of carbon atoms are sensitive indicators for secondary structure both in globular and in intrinsically disordered proteins (*45*). In the case of K18-4×KXGE, these shifts show small but distinct deviations from random coil values (Figure 4 and Figure S1 in the Supporting Information). For the phosphorylation-mimic K18-4×KXGE, continuous stretches of negative secondary chemical shifts were found for residues 274−284, 305−315, and 336−345, indicative of a propensity to form β-structure. These stretches encompass the hexapeptide motifs VQIINK and VQIVYK at the beginning of the second and third repeat, known to be important for the abnormal aggregation of tau into PHFs (*8*). The

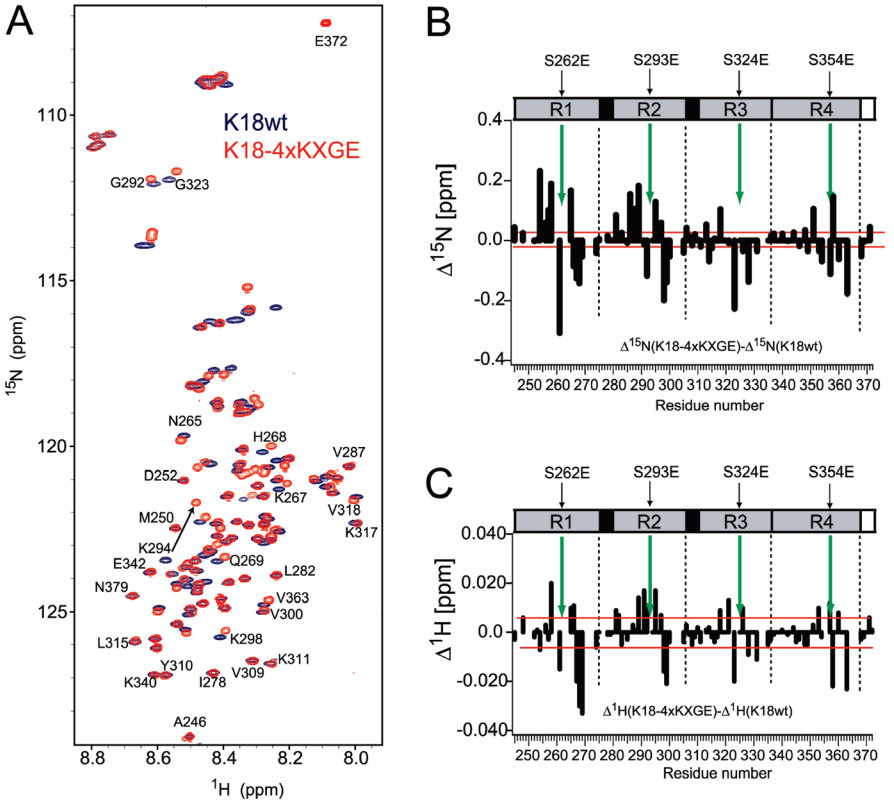

FIGURE 3: Changes in local structure induced by pseudophosphorylation. (A) Superposition of 2D HSQC spectra of K18-4×KXGE (red) and K18wt (blue). Selected sequence-specific assignments are marked. (B) Differences in ^{15}N chemical shifts between K18-4×KXGE and K18wt extracted from Figure 2A. (C) Differences in ^{1}H chemical shifts between K18-4×KXGE and K18wt extracted from Figure 2A. Horizontal lines indicate the average variation of chemical shifts observed for K18wt from sample to sample due to slightly different buffer conditions. Shift changes that exceed the red lines are regarded as significant. Gaps are due to proline residues or unassigned residues. On top, the domain organization of K18 is shown. The location of the phosphorylation-mimicking mutations (S262E, S293E, S324E, S354E) is indicated by green arrows.

secondary chemical shifts of K18-4×KXGE were very similar to those observed in the wild-type protein, with some changes in proximity to the sites of mutation (Figure 4 and Figure S1 in the Supporting Information) (*23*).

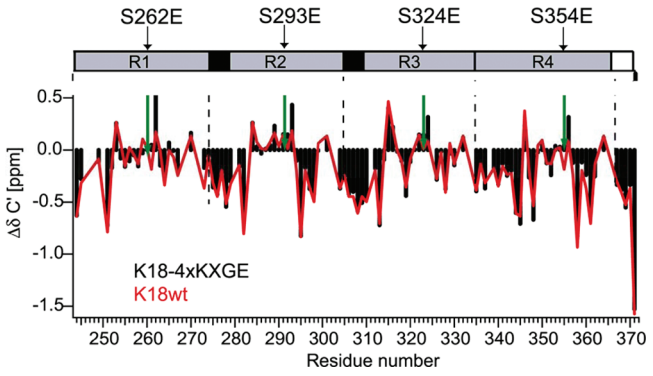

FIGURE 4: Secondary structure propensity in K18-4×KXGE. C′ secondary chemical shifts in K18-4×KXGE (black) and in K18wt (red) at 5 °C in 50 mM phosphate buffer, pH 6.9. The positions of the Ser to Glu mutations are indicated by arrows. All glycine residues at positions 2 and 3 in the PGGG motifs exhibited identical secondary chemical shifts. Secondary chemical shifts in K18-4×KXGE (black) and in K18wt (red) are very similar with some changes in the direct vicinity to the sites of mutation.

To obtain further insight into residual structure, we measured one-bond N−H residual dipolar couplings (RDCs) in K18-4×KXGE, which had been partially oriented in a Pf1 bacteriophage alignment medium. In an anisotropic environment, like magnetically oriented Pf1 phage, the large one-bond internuclear dipolar interactions no longer average to zero (for a review see ref *46*). In contrast to the bell-like smooth distribution of dipolar couplings, which is expected for random flight chains (*47*), a very specific distribution of positive and negative couplings was observed for K18-4×KXGE (Figure 5A). Four residue stretches with large positive RDC values were evident: ^{250}MPD^{252} (in repeat R1), ^{256}VKSK^{259} (in repeat R1), ^{274}KVQIINKKLDL^{284}, and ^{306}VQIVYKPVD^{314}. Regions 274−284 and 306−314 correlate well with the elements of high β-structure propensity at the beginning of R2 and R3, as identified by NMR secondary chemical shifts (Figure 4). The regions with large positive RDC values end with residues displaying negative RDCs: Lys^{254}, Ser^{285}, Asn^{286}, Ser^{316}, and Lys^{317}. We previously proposed that they are involved in turn structures (*23*, *24*). The most pronounced differences in the RDC profiles of K18-4×KXGE and K18wt were located in repeat R1 and at the beginning of repeat

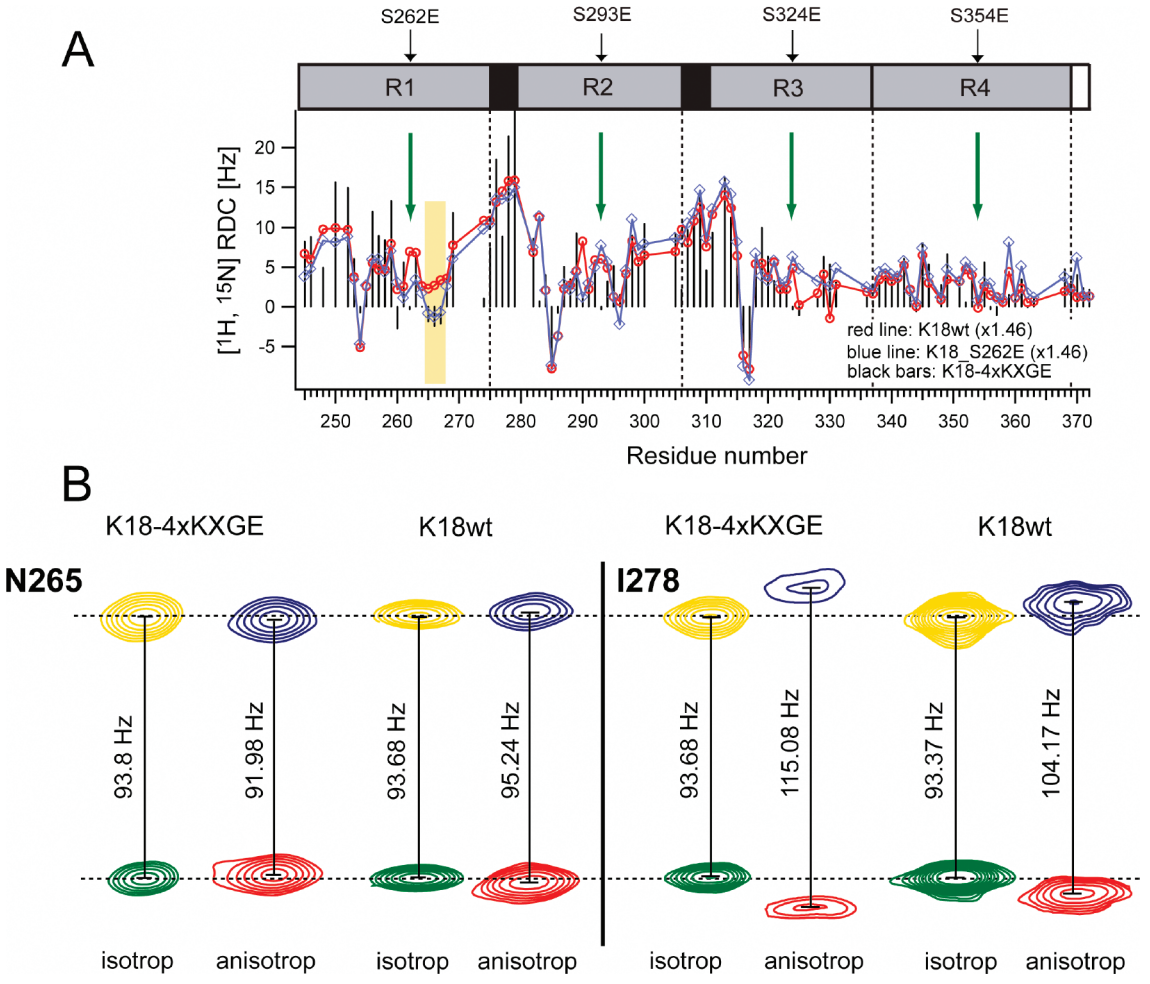

FIGURE 5: Residual dipolar couplings in K18-4×KXGE. (A) One-bond [^{1}H,^{15}N] residual dipolar couplings observed in K18-4×KXGE (black), K18-S262E (blue), and K18wt (red) aligned in Pf1 phages at 5 °C. Positive RDC values are characteristic for higher backbone rigidity and extended or β-structure, as seen for the two hexapeptide motifs in R2 and R3. Negative RDC values indicate helical or turn propensity. The yellow box highlights the sign inversion of the RDCs of residues 265−267 induced by the Ser to Glu mutations. Green arrows indicate the sites of mutation. The estimated error for RDCs is 0.2 Hz. For better comparison, RDC values of K18wt were multiplied by 1.46. (B) Isotropic (green and yellow) and anisotropic (red and blue) doublet components of Asn^{265} (left part) and Ile^{278} (right part) extracted from 2D IPAP-HSQCs recorded on K18-4×KXGE and K18wt. Coupling values are indicated.

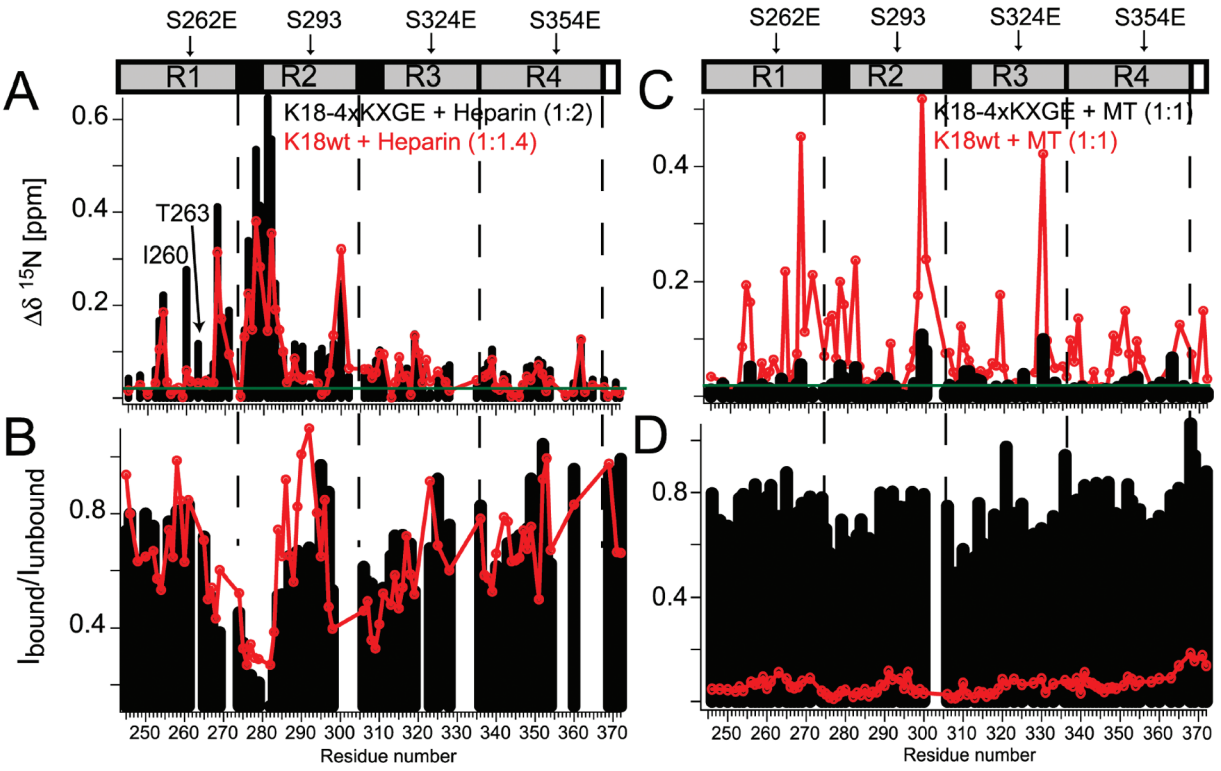

FIGURE 6: Impact of pseudophosphorylation on the interaction of the repeat domain of tau with MTs and the aggregation-inducer heparin. (A, B) Heparin-induced changes in ^{15}N chemical shifts (A) and signal intensities (B) in K18-4×KXGE (black) and in K18wt (red). Signal intensity changes are shown as the ratio between signal intensities in 2D $^{1}H-^{15}N$ HSQC spectra in the absence and presence of heparin. The concentration of tau was 150 μM, the molar tau:heparin ratios were ~1:2 for K18-4×KXGE and ~1:1.4 for K18wt. A horizontal line indicates the average variation of chemical shifts observed between different samples containing K18:heparin (4:1). Regions with large chemical shift changes and small intensity ratios are involved in the K18:heparin interaction. (C, D) Changes in ^{15}N chemical shifts (C) and signal intensities (D) in K18-4×KXGE (black) and in K18wt (red) upon addition of MTs. The molar tau:MT ratio was 1:1. Gaps are due to signal overlap or the presence of prolines. Note the strong difference in MT-induced signal broadening between K18-4×KXGE and K18wt.

R2 (Figure 5A). In the hexapeptide ^{306}VQIVYK^{311} at the beginning of R2, RDC values were increased for K18-4×KXGE, suggesting a higher rigidity. In addition, the sign of RDC values of residues ^{265}NLK^{267} was inverted in K18-4×KXGE when compared to the wild-type protein (Figure 5A,B). Sign inversions of RDCs in intrinsically disordered proteins indicate formation of turn or helical conformations (*24*, *48*) or changes in the local alignment tensor (*49*). We also tried to obtain further support for conformational changes from H^N-H^N and H^N-H^α NOEs, which was however not possible due to severe signal overlap in three-dimensional ^{15}N NOESY-HSQC spectra.

Is pseudophosphorylation at S262 sufficient for the conformational change? To answer this question, we have prepared the repeat domain of tau, in which only S262 was mutated into glutamic acid (K18-S262E). Comparison of two-dimensional $^{1}H-^{15}N$ HSQC spectra between K18wt and K18-S262E showed that chemical shift changes in repeat R1 are similar to those observed for K18-4×KXGE (Figure S2 in the Supporting Information). In contrast, chemical shift changes in repeats R2 to R4 are strongly reduced when compared to K18-4×KXGE. Next, we measured one-bond N−H RDCs in K18-S262E, which had been partially oriented in Pf1 phage (Figure 5A). When compared to K18-4×KXGE, slightly smaller RDCs are observed for residues in regions 250−260 and 276−279 in K18-S262E, and RDC values in this region are more similar to K18wt. However, RDC values of residues ^{265}NLK^{267} are inverted compared to K18wt and as observed in K18-4×KXGE, indicating that pseudophosphorylation at S262 is sufficient for turn formation at ^{265}NLK^{267}.

Influence of Pseudophosphorylation on the Interaction of the Repeat Domain of Tau with Polyanions. To identify the residues, which are important for binding to the aggregation-inducer heparin, we probed the heparin−K18-4×KXGE interaction using two-dimensional $^{1}H-^{15}N$ HSQC spectra. For K18-4×KXGE, large chemical shift changes were present for residues V275−L284, the hexapeptide motif in the beginning of repeat 2 (black bars in Figure 6A). In addition, chemical shifts of selected lysine and histidine residues (^{253}LK^{254}, ^{259}KI^{260}, ^{268}HN^{269}, and H^{299}) were affected by the addition of heparin. Overall, the pattern of heparin-induced chemical shift changes observed for K18-4×KXGE was very similar to the one previously reported for K18wt (red line in Figure 6A) (*23*). In addition, the overall magnitude of chemical shift changes was comparable (taking into account the slightly different concentrations of heparin). The chemical shift changes were accompanied by site-specific decreases in NMR signal intensities, indicating chemical exchange, which is intermediate on the NMR time scale (Figure 6B). In particular, residues in the two hexapeptide motifs (V275−L282 and V306−T319) were attenuated, consistent with their involvement in the binding process (*23*, *25*). In comparison to the wild-type protein, however, the signal intensities of residues Q^{269}, K^{274}, and ^{289}SKCGS^{293} were more strongly broadened, suggesting an increased contribution from chemical exchange.

Binding of the Repeat Domain of Tau to Microtubules: Influence of Pseudophosphorylation. The binding of full-length tau to MTs occurs in two structurally and kinetically distinct steps, comprising a first binding phase with low

stoichiometry but tight binding (K_d 0.1 μM) and a second phase of weaker affinity but higher and nonsaturable stoichiometry (*50*). Here we probed the binding of K18-4×KXGE to paclitaxel-stabilized MTs using two-dimensional $^1H-^{15}N$ HSQC spectra. From a solution-state NMR perspective, tau in the MT-bound state is invisible due to the very fast relaxation of the NMR signals. However, we previously showed that chemical shift changes and exchange-induced broadening of specific regions of tau can be observed in the presence of MTs and thus allows identification of the hot spots of the tau−MT interaction (*3*, *23*). Moreover, we had demonstrated that at higher ionic strength, at which the MT-binding strength of tau is reduced and the weaker, nonsaturable MT-binding is strongly attenuated, the pattern of MT-induced chemical shift changes is very similar, indicating that the NMR assay reports on the primary, strong binding of tau to microtubules (*25*, *51*). Addition of MTs to K18-4×KXGE (molar tau:MT ratio of 1:1) induced only very small chemical shift changes, in clear contrast to K18wt (Figure 6C). In addition, NMR signal intensities were only slightly reduced, although lower signal intensities were still visible for the two hexapeptides in repeats R2 and R3 (Figure 6D). Comparison with K18wt (red line in Figure 6D) demonstrates that pseudophosphorylation of the repeat domain results in a much larger fraction of unbound tau.

DISCUSSION

Phosphorylation is the decisive factor governing the biological and pathological function of tau. Here we have characterized the structural consequences and the effect on binding to polyanions and microtubules of the repeat region of tau (K18), when it carries four mutations (S262E, S293E, S324E, S356E) that mimic phosphorylation of the sequential motifs KIGS and KCGS at these sites. The major results can be summarized as follows: (1) Glutamate mutations, mimicking the phosphorylation at KXGS motifs in the repeat domain, do not significantly influence the secondary structure propensity of K18 in its monomeric state in solution. However, they induce selective conformational changes in the first and second repeat, in particular for residues ^{265}NLK^{267}. (2) The interaction with the aggregation-inducer heparin remains largely unchanged by phosphorylation mimics. (3) The mutations significantly attenuate binding to microtubules. (4) The striking difference in the effect of the phosphorylation-mimicking mutations on the heparin−tau and MT−tau interactions highlights the specificity and tight regulation of the binding of tau to MTs.

Serine to Glutamic Acid Mutations Induce Selective Structural Changes in Proximity to S262. NMR chemical shifts of backbone resonances allow a sensitive detection of structural changes. The repeat region of four-repeat tau consists of four pseudorepeats with about 31 residues each (Figure 1). Surprisingly, the magnitude of changes in chemical shifts and residual dipolar couplings induced by the four mutations (S262E in R1, S293E in R2, S324E in R3, and S356E in R4) is not the same in the four repeats. The most pronounced differences in the chemical shift and RDC profiles of K18-4×KXGE and K18wt were observed in repeats R1 and R2. In particular, the RDC values of K18-4×KXGE were changed in repeat R1 and in the hexapeptide at the beginning of R2. Only in repeat R1 was an inversion of the sign of RDC values observed. The sign inversion occurred for residues ^{265}NLK^{267} and suggests formation of a turn-like structure by residues ^{265}NLK^{267} upon pseudophosphorylation of the repeat region of tau (*24*). Importantly, ^{265}NLK^{267} is in close proximity to S262, the phosphorylation site that most strongly attenuates binding to MTs (*14*). Moreover, ^{265}NLK^{267} is upstream of the hexapeptide in the beginning of R2, which is important for both aggregation of tau into PHFs and binding of tau to MTs (*3*, *8*).

What makes repeat R1 so special? Close inspection of the primary sequence of the repeat region of tau reveals that upstream of residues ^{265}NLK^{267} a negative charge is found (^{261}GSTE^{264}) while downstream of it one to two (depending on pH) positive charges are found (^{267}KHQ^{269}). In addition, three lysine residues are located in the beginning of repeat R2 (K^{274}, K^{280}, K^{281}), which represent a hot spot of microtubule binding (*5*). Thus, phosphorylation at S^{262} might tighten an electrostatic interaction between the KIGS motif in repeat R1 and the end of R1/beginning of R2. This could reduce the ability for intermolecular interactions of the ^{275}VQIINK^{280} hexapeptide, in agreement with the finding that phosphorylation of tau at S^{262} inhibits aggregation of tau into PHFs (*52*). In contrast, downstream of the other three phosphorylation sites (S^{293} in R2, S^{324} in R3, and S^{356} in R4) a smaller excess of positively charged residues is present: ^{298}KH^{299} and K^{311} downstream of S^{293}; ^{329}HHK^{331} and ^{338}EVKSEK^{343} downstream of S^{324}; H^{362} and ^{369}KKIE^{372} downstream of S^{356}. Interestingly, the familial L266 V mutation, which causes frontotemporal dementia and is part of the ^{265}NLK^{267} stretch, shows a reduced ability to promote microtubule assembly (*53*).

The Binding of the Repeat Domain of Tau to Microtubules Is Highly Specific in Contrast to the Tau−Polyanion Interaction. Tau is a microtubule-associated protein that regulates diverse and essential MT functions, including polymerization and stabilization of MTs and modulation of MT dynamics (*4*). The domains flanking the repeat region bind strongly to MTs, even in the absence of the repeats, whereas the repeat motifs are essential for MT assembly (*54*). Three out of the four MT-binding hot spots of tau are located in the repeat domain of tau (^{245}TAPVPMPDL^{253} in repeat R1, ^{275}VQIINKKLDLSNV^{287} in repeat R2, and ^{306}VQIVYKPVDLSKV^{318} in repeat R3) (*3*, *5*). Phosphorylation in the repeat region of tau is known to weaken the interaction of tau with MTs and cause a decrease in MT stabilization (*14*). Therefore, insight into the detailed mechanism by which phosphorylation affects the ability of tau to bind to MTs is important.

Our NMR analysis demonstrates that pseudophosphorylation of the repeat domain strongly attenuates binding of tau to MTs (Figure 6C,D). Previous studies have shown that in particular phosphorylation of Ser^{262} decreases the tau−MT affinity (*14*). As discussed above, the most pronounced conformational changes upon pseudophosphorylation of the repeat domain were observed in close proximity to Ser^{262}. The combined data suggest that the conformational changes observed by NMR for tau in solution are responsible for the strong impact of phosphorylation at Ser^{262} on the tau−MT interaction: when Ser^{262} is phosphorylated, a turn conformation is induced that is no longer compatible with the structural changes required for efficient binding to MTs (Figure 7). In agreement with this hypothesis is the observation that Ser^{262} is located in between the two central MT-binding hot spots (^{245}TAPVPMPDL^{253} and ^{275}VQIINKKLDLSNV^{287}) (*3*). To allow for efficient binding of the two regions to MTs, structural rearrangements in the intervening residue stretch, comprising Ser^{262}, are likely to be required.

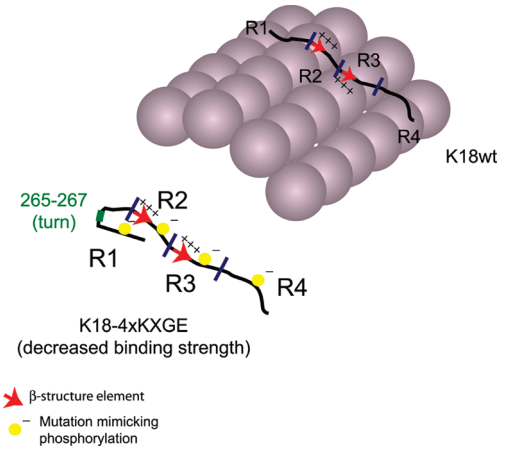

FIGURE 7: Model for the conformational changes induced by pseudophosphorylation of the repeat domain of tau. Wild-type tau can bind to microtubules, whereas the mutated construct (phosphate groups are shown as yellow dots) can no longer bind, due to the formation of a turn and the resulting contact between repeats R1 and R2, which interferes with MT binding.

Polyanions such as heparin are often used to accelerate the assembly of tau into PHFs (*55*, *56*). Our data demonstrate that, in contrast to MT binding, the tau−heparin interaction is not strongly affected by pseudophosphorylation in the repeat domain (Figure 6). This is surprising as it was previously shown that phosphorylation at S262 interferes with heparin-induced assembly of tau into PHFs *in vitro* (*52*). On the other hand, it was also demonstrated that heparin accelerates aggregation of tau but is not incorporated into PHF (*23*, *57*), indicating that it mostly enhances the formation of aggregation nuclei but is not essential for stabilization of PHFs. As our data indicate that the tau−heparin interaction is not strongly affected, phosphorylation in the repeat domain most likely interferes with the structural changes that occur during formation of PHFs. In agreement with this hypothesis, solid-state NMR spectroscopy revealed that S262 is located at the beginning of a β-strand in the fibrillar core of PHFs (*7*). At the same time, however, the surprising finding remains that phosphorylation sites such as S262, which block phosphorylation of tau into PHFs *in vitro* (*52*), are to some extent (~30%) accessible for phosphorlyation in the PHF structure *in vitro* (*52*) and are prominent phosphorylation sites in Alzheimer PHF as identified by mass spectrometry (*58*). This is resolved when we consider that amyloid fibrils are dynamic entities, for which recycling of molecules within the fibril population occurs continuously (*59*). Another possibility is that, in AD, proteolytic fragments of tau representing the repeat domain are generated which can nucleate PHFs and whose assembly is less sensitive to phosphorylation (*52*).

The binding of the repeat domain of tau to polyanions and to paclitaxel-stabilized MTs involves similar residues (*23*, *25*). In agreement with this finding, poly(Glu) peptides were thought to resemble the Glu-rich C-terminal sequence of tubulin, and it is commonly accepted that tau interacts with the highly negatively charged C-terminus of tubulin that is believed to be exposed on the surface of MTs (*60*). The data presented here, however, revealed that pseudophosphorylation of the repeat domain has only a minor effect on the interaction with the polyanion heparin but strongly reduces the binding to MTs. This strongly questions the use of poly(Glu) as a tool to study the interaction of tau with MTs. Even more important, our data demonstrate that the interaction of tau with microtubules is highly specific (Figure 7). The difference in the topology of negative charges on MTs and heparin may explain such discrimination when heparin with a dense charge repartition is still able to interact with clusters of charges on tau while the binding of tau to the C-terminal domain of tubulin in the MTs would require a specific spacing between different parts of tau. Moreover, a recent study on full-length tau indicated that binding of tau to MTs is not driven purely by electrostatic interactions, as the hot spots of the tau−MT interaction comprise many hydrophobic residues (*3*). In summary, our data show that subtle but specific conformational changes in the intrinsically disordered protein tau can have a strong impact on its biological function and involvement in disease.

ACKNOWLEDGMENT

We thank Eva-Maria Mandelkow for stimulating discussions and Alice Soragni for preliminary experiments.

SUPPORTING INFORMATION AVAILABLE

C^{α} secondary chemical shifts in K18-4×KXGE (black) and in K18wt (red) and ^{15}N chemical shift differences between K18-4×KXGE and K18wt (black bars) and between K18-S262E and K18wt (red bars). This material is available free of charge via the Internet at http://pubs.acs.org.

REFERENCES

1. Braak, H., and Braak, E. (1991) Neuropathological staging of Alzheimer-related changes. *Acta Neuropathol. 82*, 239–259.
2. Santacruz, K., Lewis, J., Spires, T., Paulson, J., Kotilinek, L., Ingelsson, M., Guimaraes, A., DeTure, M., Ramsden, M., McGowan, E., Forster, C., Yue, M., Orne, J., Janus, C., Mariash, A., Kuskowski, M., Hyman, B., Hutton, M., and Ashe, K. H. (2005) Tau suppression in a neurodegenerative mouse model improves memory function. *Science 309*, 476–481.
3. Mukrasch, M. D., Bibow, S., Korukottu, J., Jeganathan, S., Biernat, J., Griesinger, C., Mandelkow, E., and Zweckstetter, M. (2009) Structural polymorphism of 441-residue tau at single residue resolution. *PLoS Biol. 7*, e34.
4. Gustke, N., Trinczek, B., Biernat, J., Mandelkow, E. M., and Mandelkow, E. (1994) Domains of tau protein and interactions with microtubules. *Biochemistry 33*, 9511–9522.
5. Goode, B. L., and Feinstein, S. C. (1994) Identification of a novel microtubule binding and assembly domain in the developmentally regulated inter-repeat region of tau. *J. Cell Biol. 124*, 769–782.
6. Wischik, C. M., Novak, M., Edwards, P. C., Klug, A., Tichelaar, W., and Crowther, R. A. (1988) Structural characterization of the core of the paired helical filament of Alzheimer disease. *Proc. Natl. Acad. Sci. U.S.A. 85*, 4884–4888.
7. Andronesi, O. C., von Bergen, M., Biernat, J., Seidel, K., Griesinger, C., Mandelkow, E., and Baldus, M. (2008) Characterization of Alzheimer's-like paired helical filaments from the core domain of tau protein using solid-state NMR spectroscopy. *J. Am. Chem. Soc. 130*, 5922–5928.
8. von Bergen, M., Friedhoff, P., Biernat, J., Heberle, J., Mandelkow, E. M., and Mandelkow, E. (2000) Assembly of tau protein into Alzheimer paired helical filaments depends on a local sequence motif ((306)VQIVYK(311)) forming beta structure. *Proc. Natl. Acad. Sci. U.S.A. 97*, 5129–5134.
9. Mi, K., and Johnson, G. V. (2006) The role of tau phosphorylation in the pathogenesis of Alzheimer's disease. *Curr. Alzheimer Res. 3*, 449–463.
10. Bancher, C., Brunner, C., Lassmann, H., Budka, H., Jellinger, K., Seitelberger, F., Grundke-Iqbal, I., Iqbal, K., and Wisniewski, H. M. (1989) Tau and ubiquitin immunoreactivity at different stages of formation of Alzheimer neurofibrillary tangles. *Prog. Clin. Biol. Res. 317*, 837–848.
11. Kopke, E., Tung, Y. C., Shaikh, S., Alonso, A. C., Iqbal, K., and Grundke-Iqbal, I. (1993) Microtubule-associated protein tau. Abnormal phosphorylation of a non-paired helical filament pool in Alzheimer disease. *J. Biol. Chem. 268*, 24374–24384.
12. Braak, H., and Braak, E. (1994) Morphological criteria for the recognition of Alzheimer's disease and the distribution pattern of

cortical changes related to this disorder. *Neurobiol. Aging 15*, 355–356 (discussion 379−380).
13. Wittmann, C. W., Wszolek, M. F., Shulman, J. M., Salvaterra, P. M., Lewis, J., Hutton, M., and Feany, M. B. (2001) Tauopathy in *Drosophila*: neurodegeneration without neurofibrillary tangles. *Science 293*, 711–714.
14. Biernat, J., Gustke, N., Drewes, G., Mandelkow, E. M., and Mandelkow, E. (1993) Phosphorylation of Ser262 strongly reduces binding of tau to microtubules: distinction between PHF-like immunoreactivity and microtubule binding. *Neuron 11*, 153–163.
15. Drewes, G., Trinczek, B., Illenberger, S., Biernat, J., Schmitt-Ulms, G., Meyer, H. E., Mandelkow, E. M., and Mandelkow, E. (1995) Microtubule-associated protein/microtubule affinity-regulating kinase (p110mark). A novel protein kinase that regulates tau-microtubule interactions and dynamic instability by phosphorylation at the Alzheimer-specific site serine 262. *J. Biol. Chem. 270*, 7679–7688.
16. Augustinack, J. C., Schneider, A., Mandelkow, E. M., and Hyman, B. T. (2002) Specific tau phosphorylation sites correlate with severity of neuronal cytopathology in Alzheimer's disease. *Acta Neuropathol. (Berlin) 103*, 26–35.
17. Chin, J. Y., Knowles, R. B., Schneider, A., Drewes, G., Mandelkow, E. M., and Hyman, B. T. (2000) Microtubule-affinity regulating kinase (MARK) is tightly associated with neurofibrillary tangles in Alzheimer brain: a fluorescence resonance energy transfer study. *J. Neuropathol. Exp. Neurol. 59*, 966–971.
18. Mocanu, M. M., Nissen, A., Eckermann, K., Khlistunova, I., Biernat, J., Drexler, D., Petrova, O., Schonig, K., Bujard, H., Mandelkow, E., Zhou, L., Rune, G., and Mandelkow, E. M. (2008) The potential for beta-structure in the repeat domain of tau protein determines aggregation, synaptic decay, neuronal loss, and coassembly with endogenous Tau in inducible mouse models of tauopathy. *J. Neurosci. 28*, 737–748.
19. Cleveland, D. W., Hwo, S. Y., and Kirschner, M. W. (1977) Physical and chemical properties of purified tau factor and the role of tau in microtubule assembly. *J. Mol. Biol. 116*, 227–247.
20. Dyson, H. J., and Wright, P. E. (2005) Intrinsically unstructured proteins and their functions. *Nat. Rev. Mol. Cell. Biol. 6*, 197–208.
21. Eliezer, D., Barre, P., Kobaslija, M., Chan, D., Li, X., and Heend, L. (2005) Residual structure in the repeat domain of tau: echoes of microtubule binding and paired helical filament formation. *Biochemistry 44*, 1026–1036.
22. Fischer, D., Mukrasch, M. D., von Bergen, M., Klos-Witkowska, A., Biernat, J., Griesinger, C., Mandelkow, E., and Zweckstetter, M. (2007) Structural and microtubule binding properties of tau mutants of frontotemporal dementias. *Biochemistry 46*, 2574–2582.
23. Mukrasch, M. D., Biernat, J., von Bergen, M., Griesinger, C., Mandelkow, E., and Zweckstetter, M. (2005) Sites of TAU important for aggregation populate beta-structure and bind to microtubules and polyanions. *J. Biol. Chem. 280*, 24978–24986.
24. Mukrasch, M. D., Markwick, P., Biernat, J., Bergen, M., Bernado, P., Griesinger, C., Mandelkow, E., Zweckstetter, M., and Blackledge, M. (2007) Highly populated turn conformations in natively unfolded tau protein identified from residual dipolar couplings and molecular simulation. *J. Am. Chem. Soc. 129*, 5235–5243.
25. Mukrasch, M. D., von Bergen, M., Biernat, J., Fischer, D., Griesinger, C., Mandelkow, E., and Zweckstetter, M. (2007) The "jaws" of the tau-microtubule interaction. *J. Biol. Chem. 282*, 12230–12239.
26. Sillen, A., Barbier, P., Landrieu, I., Lefebvre, S., Wieruszeski, J. M., Leroy, A., Peyrot, V., and Lippens, G. (2007) NMR investigation of the interaction between the neuronal protein tau and the microtubules. *Biochemistry 46*, 3055–3064.
27. Sillen, A., Wieruszeski, J. M., Leroy, A., Younes, A. B., Landrieu, I., and Lippens, G. (2005) High-resolution magic angle spinning NMR of the neuronal tau protein integrated in Alzheimer's-like paired helical fragments. *J. Am. Chem. Soc. 127*, 10138–10139.
28. Sibille, N., Sillen, A., Leroy, A., Wieruszeski, J. M., Mulloy, B., Landrieu, I., and Lippens, G. (2006) Structural impact of heparin binding to full-length Tau as studied by NMR spectroscopy. *Biochemistry 45*, 12560–12572.
29. Du, J. T., Li, Y. M., Ma, Q. F., Qiang, W., Zhao, Y. F., Abe, H., Kanazawa, K., Qin, X. R., Aoyagi, R., Ishizuka, Y., Nemoto, T., and Nakanishi, H. (2005) Synthesis and conformational properties of phosphopeptides related to the human tau protein. *Regul. Pept. 130*, 48–56.
30. Daly, N. L., Hoffmann, R., Otvos, L., and Craik, D. J. (2000) Role of phosphorylation in the conformation of tau peptides implicated in Alzheimer's disease. *Biochemistry 39*, 9039–9046.
31. Bielska, A. A., and Zondlo, N. J. (2006) Hyperphosphorylation of tau induces local polyproline II helix. *Biochemistry 45*, 5527–5537.
32. Smet, C., Sambo, A. V., Wieruszeski, J. M., Leroy, A., Landrieu, I., Buee, L., and Lippens, G. (2004) The peptidyl prolyl cis/trans-isomerase Pin1 recognizes the phospho-Thr212-Pro213 site on Tau. *Biochemistry 43*, 2032–2040.
33. Fath, T., Eidenmuller, J., and Brandt, R. (2002) Tau-mediated cytotoxicity in a pseudohyperphosphorylation model of Alzheimer's disease. *J. Neurosci. 22*, 9733–9741.
34. Rankin, C. A., Sun, Q., and Gamblin, T. C. (2005) Pseudo-phosphorylation of tau at Ser202 and Thr205 affects tau filament formation. *Brain Res. Mol. Brain Res. 138*, 84–93.
35. Delaglio, F., Grzesiek, S., Vuister, G. W., Zhu, G., Pfeifer, J., and Bax, A. (1995) NMRPipe: a multidimensional spectral processing system based on UNIX pipes. *J. Biomol. NMR 6*, 277–293.
36. Vuister, G. W., and Bax, A. (1993) Quantitative J correlation: a new approach for measuring homonuclear 3-bond J(H(N)H(alpha) coupling constants in N-15-enriched proteins. *J. Am. Chem. Soc. 115*, 7772–7777.
37. Zuiderweg, E. R. P., and Fesik, S. W. (1989) Heteronuclear 3-dimensional NMR spectroscopy of the inflammatory protein C5A. *Biochemistry 28*, 2387–2391.
38. Grzesiek, S., and Bax, A. (1992) Improved 3D triple-resonance NMR techniques applied to a 31-kDa protein. *J. Magn. Reson. 96*, 432–440.
39. Johnson, B. A., and Blevins, R. A. (1994) Nmr View—a computer program for the visualization and analysis of NMR data. *J. Biomol. NMR 4*, 603–614.
40. Schwarzinger, S., Kroon, G. J., Foss, T. R., Chung, J., Wright, P. E., and Dyson, H. J. (2001) Sequence-dependent correction of random coil NMR chemical shifts. *J. Am. Chem. Soc. 123*, 2970–2978.
41. Wishart, D. S., and Sykes, B. D. (1994) Chemical shifts as a tool for structure determination. *Methods Enzymol. 239*, 363–392.
42. Wishart, D. S., Bigam, C. G., Holm, A., Hodges, R. S., and Sykes, B. D. (1995) H-1, C-13 and N-15 random coil NMR chemical shifts of the common amino acids. 1. Investigations of nearest-neighbor effects. *J. Biomol. NMR 5*, 67–81.
43. Tjandra, N., and Bax, A. (1997) Direct measurement of distances and angles in biomolecules by NMR in a dilute liquid crystalline medium. *Science 278*, 1111–1114.
44. Ottiger, M., Delaglio, F., and Bax, A. (1998) Measurement of J and dipolar couplings from simplified two-dimensional NMR spectra. *J. Magn. Reson. 131*, 373–378.
45. Wright, P. E., and Dyson, H. J. (1999) Intrinsically unstructured proteins: re-assessing the protein structure-function paradigm. *J. Mol. Biol. 293*, 321–331.
46. Bax, A., and Grishaev, A. (2005) Weak alignment NMR: a hawk-eyed view of biomolecular structure. *Curr. Opin. Struct. Biol. 15*, 563–570.
47. Louhivuori, M., Paakkonen, K., Fredriksson, K., Permi, P., Lounila, J., and Annila, A. (2003) On the origin of residual dipolar couplings from denatured proteins. *J. Am. Chem. Soc. 125*, 15647–15650.
48. Mohana-Borges, R., Goto, N. K., Kroon, G. J., Dyson, H. J., and Wright, P. E. (2004) Structural characterization of unfolded states of apomyoglobin using residual dipolar couplings. *J. Mol. Biol. 340*, 1131–1142.
49. Skora, L., Cho, M. K., Kim, H. Y., Becker, S., Fernandez, C. O., Blackledge, M., and Zweckstetter, M. (2006) Charge-induced molecular alignment of intrinsically disordered proteins. *Angew. Chem., Int. Ed. Engl. 45*, 7012–7015.
50. Ackmann, M., Wiech, H., and Mandelkow, E. (2000) Nonsaturable binding indicates clustering of tau on the microtubule surface in a paired helical filament-like conformation. *J. Biol. Chem. 275*, 30335–30343.
51. Fischer, M. B., Roeckl, C., Parizek, P., Schwarz, H. P., and Aguzzi, A. (2000) Binding of disease-associated prion protein to plasminogen. *Nature 408*, 479–483.
52. Schneider, A., Biernat, J., von Bergen, M., Mandelkow, E., and Mandelkow, E. M. (1999) Phosphorylation that detaches tau protein from microtubules (Ser262, Ser214) also protects it against aggregation into Alzheimer paired helical filaments. *Biochemistry 38*, 3549–3558.
53. Kobayashi, T., Ota, S., Tanaka, K., Ito, Y., Hasegawa, M., Umeda, Y., Motoi, Y., Takanashi, M., Yasuhara, M., Anno, M., Mizuno, Y., and Mori, H. (2003) A novel L266 V mutation of the tau gene causes frontotemporal dementia with a unique tau pathology. *Ann. Neurol. 53*, 133–137.
54. Preuss, U., Biernat, J., Mandelkow, E. M., and Mandelkow, E. (1997) The "jaws" model of tau-microtubule interaction examined in CHO cells. *J. Cell. Sci. 110* (Part 6), 789–800.

55. Kampers, T., Friedhoff, P., Biernat, J., Mandelkow, E. M., and Mandelkow, E. (1996) RNA stimulates aggregation of microtubule-associated protein tau into Alzheimer-like paired helical filaments. *FEBS Lett. 399*, 344–349.
56. Goedert, M., Spillantini, M. G., Hasegawa, M., Jakes, R., Crowther, R. A., and Klug, A. (1996) Molecular dissection of the neurofibrillary lesions of Alzheimer's disease. *Cold Spring Harbor Symp. Quant. Biol. 61*, 565–573.
57. von Bergen, M., Barghorn, S., Muller, S. A., Pickhardt, M., Biernat, J., Mandelkow, E. M., Davies, P., Aebi, U., and Mandelkow, E. (2006) The core of tau-paired helical filaments studied by scanning transmission electron microscopy and limited proteolysis. *Biochemistry 45*, 6446–6457.
58. Morishima-Kawashima, M., Hasegawa, M., Takio, K., Suzuki, M., Yoshida, H., Titani, K., and Ihara, Y. (1995) Proline-directed and non-proline-directed phosphorylation of PHF-tau. *J. Biol. Chem. 270*, 823–829.
59. Carulla, N., Caddy, G. L., Hall, D. R., Zurdo, J., Gairi, M., Feliz, M., Giralt, E., Robinson, C. V., and Dobson, C. M. (2005) Molecular recycling within amyloid fibrils. *Nature 436*, 554–558.
60. Downing, K. H., and Nogales, E. (1998) Tubulin structure: insights into microtubule properties and functions. *Curr. Opin. Struct. Biol. 8*, 785–791.